

See discussions, stats, and author profiles for this publication at: <https://www.researchgate.net/publication/7396551>

Preparation and Nonlinear Optical Properties of Inorganic–Organic Hybrid Films with Various Substituents on Chromophores

ARTICLE *in* THE JOURNAL OF PHYSICAL CHEMISTRY B · JANUARY 2006

Impact Factor: 3.3 · DOI: 10.1021/jp0549677 · Source: PubMed

CITATIONS

19

READS

12

6 AUTHORS, INCLUDING:



Yuanjing Cui

Zhejiang University

117 PUBLICATIONS 3,674 CITATIONS

SEE PROFILE



Junkuo Gao

Zhejiang Sci-Tech University

59 PUBLICATIONS 1,244 CITATIONS

SEE PROFILE



Zhiyu Wang

Zhejiang University

163 PUBLICATIONS 1,962 CITATIONS

SEE PROFILE

Preparation and Nonlinear Optical Properties of Inorganic–Organic Hybrid Films with Various Substituents on Chromophores

Yuanjing Cui, Guodong Qian,* Junkuo Gao, Lujian Chen, Zhiyu Wang, and Minquan Wang

Department of Materials Science and Engineering, State Key Lab of Silicon Materials, Zhejiang University, Hangzhou 310027, PR China

Received: September 1, 2005; In Final Form: October 6, 2005

Four kinds of hydroxy-ended azobenzene-type chromophores containing different substituent groups as electron donor or electron acceptor were synthesized and further reacted with 3-isocyanatopropyltriethoxysilane (ICTES) to give alkoxysilane dyes via a urethane reaction. Following a sol–gel process of the alkoxysilane dyes, the inorganic–organic hybrid nonlinear optical (NLO) films were successfully prepared. Molecular structures of the resultant films were confirmed by elemental analysis, FTIR, and ^1H NMR. The $\beta_{\text{CT}}\mu_{\text{g}}$ values of the chromophores were evaluated by a solvatochromic method, and the second harmonic coefficients (d_{33}) of the hybrid films were measured by in situ second harmonic generation (SHG) measurement. The hybrid films exhibited large optical nonlinearity and full transparency in the visible range. The effects of substituent group and position on $\beta_{\text{CT}}\mu_{\text{g}}$ values of the chromophores and d_{33} values of the films were also discussed.

Introduction

Organic poled polymers offer great promise for the fabrication of integrated optical devices due to their large electrooptic coefficients, low dielectric constants, and ease of fabrication.^{1–7} For the practical application of second-order nonlinear optical (NLO) polymeric materials, high NLO activities and temporal and thermal stabilities are particularly required. The inorganic–organic hybrid materials exhibit dual functionality as inorganic glass and organic polymer. Therefore, they have the potential for excellent optical nonlinearity, good mechanical properties, high thermal and temporal stability, and low optical loss. A recent study on sol–gel derived inorganic–organic hybrids for second-order nonlinear optics has shown some encouraging results.^{8–11}

The optimization of molecular hyperpolarizability (β) has attracted a great deal of interest in the last years, and actually it represents an important research topic in the engineering design of highly NLO materials. Generally, chromophores containing the donor– π –acceptor (π represents an electron-conjugated bridge) charge-transfer structure exhibit large molecular hyperpolarizability (β). As an example, the azo dye Disperse Red 1 (DR1) is the most widely used chromophore, in which amino group acts as electron donor group and nitro as acceptor. In this kind of system, the electron-conjugated bridge, electron donor, and electron acceptor play important roles. Experimental studies on benzene and stilbene derivatives have demonstrated that increasing the donor and acceptor strength resulted in a steady enhancement of β and that extension of the conjugated bridge led to a pronounced increase in β value.^{12–14} These methods have attracted much attention recently, and numerous efforts have been devoted to the improvement of the molecular hyperpolarizability. However, most of the reported works were based on organic polymeric materials, and the property–structure relationship of optical nonlinearity in sol–gel derived materials received little attention.

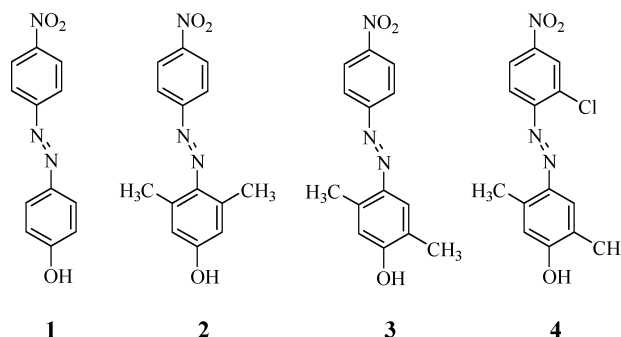


Figure 1. Chemical structures of azobenzene chromophores investigated in this study.

The chromophore 4-nitro-4'-hydroxyazobenzene has excellent transparency in the visible range, and its maximum absorption (λ_{max}) was at 380 nm, which is far away from the working wavelength of the laser source. However, the poor molecular hyperpolarizability (β) restricts its application in NLO materials. To obtain excellent NLO sol–gel materials with a good nonlinearity–transparency balance, we selected and synthesized a series of azobenzene chromophores with different substituent groups to act as electron donor or acceptor. The molecular structure of the chromophores is shown in Figure 1. Through a nucleophilic addition reaction, alkoxysilane dyes (ASD) were successfully synthesized between 3-isocyanatopropyltriethoxysilane (ICTES) and the resulting chromophores. Following a hydrolysis and condensation process of the dye-attached precursor, inorganic–organic hybrid films were obtained. The $\beta_{\text{CT}}\mu_{\text{g}}$ values for these chromophores and second harmonic coefficients (d_{33}) of the corresponding films were measured. We also discussed the influence of substituent group and substituent position on $\beta_{\text{CT}}\mu_{\text{g}}$ and d_{33} value.

Experimental Section

Materials. Tetrahydrofuran (THF) was dried by refluxing and distilled from calcium hydride just before use. ICTES was

* Corresponding author. Tel: +86-571-87952334. Fax: +86-571-87951234. E-mail address: gdqian@zju.edu.cn.

obtained from Tokyo Chemical Industry Co. and used as received. 2-Chloro-4-nitrobenzenamine was obtained from Alfa Aesar and used without further purification. All other reagents, of analytical-grade quality, were commercial products and used as received.

Synthesis of 4-Nitro-4'-hydroxy-azobenzene (Chromophore 1). 4-Nitrobenzenamine (2.76 g, 20 mmol) dissolved in 20 mL of distilled water and 18 mL of concentrated HCl was cooled to 0–5 °C, and then a solution of sodium nitrite (1.38 g, 20 mmol) in water was added dropwise with stirring. After 15 min stirring, phenol (1.98 g, 20 mmol) and NaOH (7 g) dissolved in 50 mL of methanol/water (2:1) was added with vigorous stirring for one-half hour. The precipitate formed was filtered and washed repeatedly with water to remove any remaining reactants. The product was recrystallized from ethanol/water (1:3) and dried under vacuum at 40 °C for 6 h. Yield: 86%. Mp = 219 °C. ¹H NMR (500 MHz, DMSO-*d*₆, ppm): 10.62 (s, OH, 1H), 8.41 (s, ArH, 2H), 8.01 (s, ArH, 2H), 7.89 (s, ArH, 2H), 7.01 (s, ArH, 2H). Anal. Calcd for C₁₂H₉N₃O₃ (243.1): C, 59.26; H, 3.70; N, 17.28. Found: C, 59.13; H, 3.69; N, 17.03.

Synthesis of 3,5-Dimethyl-4-(4'-nitrophenylazo)phenol (Chromophore 2) and 2,5-Dimethyl-4-(4'-nitrophenylazo)phenol (Chromophore 3). Chromophores 2 and 3 were synthesized similar to 1 by using of 3,5-dimethyl phenol and 2,5-dimethyl phenol instead of phenol, respectively.

Chromophore (2). Yield: 81%. Mp = 170 °C. ¹H NMR (500 MHz, DMSO-*d*₆, ppm): 10.27 (s, OH, 1H), 8.39 (d, ArH, 2H), 7.94 (d, ArH, 2H), 6.64 (s, ArH, 2H), 2.51 (s, CH₃, 6H). Anal. Calcd for C₁₄H₁₃N₃O₃ (271.3): C, 61.98; H, 4.83; N, 15.49. Found: C, 61.70; H, 4.86; N, 15.36.

Chromophore (3). Yield: 65%. Mp = 227 °C. ¹H NMR (500 MHz, DMSO-*d*₆, ppm): 10.45 (s, OH, 1H), 8.38 (d, ArH, 2H), 7.97 (d, ArH, 2H), 7.57 (s, ArH, 1H), 6.83 (s, ArH, 1H), 3.33 (s, CH₃, 3H), 2.14 (s, CH₃, 3H). Anal. Calcd for C₁₄H₁₃N₃O₃ (271.3): C, 61.98; H, 4.83; N, 15.49. Found: C, 61.41; H, 4.84; N, 15.10.

Synthesis of 2,5-Dimethyl-4-(2'-chloro-4'-nitrophenylazo)-phenol (Chromophore 4). 2-Chloro-4-nitrobenzenamine (3.45 g, 20 mmol) was dissolved in 10 mL of concentrated (98%) sulfuric acid in an ice bath, then treated by adding dropwise a solution of 1.4 g (20 mmol) of sodium nitrite in 20 mL of sulfuric acid under stirring and cooling. After complete addition, the 2,5-dimethyl phenol (2.44 g, 20 mmol) dissolved in 60 mL of methanol/water (2:1) was added; then the mixture was stirred for 1 h under cooling, followed by neutralization (pH 7–8) with ammonia and stirring for 2 h more. The precipitate was filtered and recrystallized from ethanol/water (1:1). Yield: 53%. Mp = 196 °C. ¹H NMR (500 MHz, DMSO-*d*₆, ppm): 10.64 (s, OH, 1H), 8.46 (d, ArH, 1H), 8.26 (m, ArH, 1H), 7.76 (d, ArH, 1H), 7.56 (s, ArH, 1H), 6.83 (s, ArH, 1H), 3.34 (s, CH₃, 3H), 2.13 (s, CH₃, 3H). Anal. Calcd for C₁₄H₁₂ClN₃O₃ (305.7): C, 55.00; H, 3.96; N, 13.74. Found: C, 54.96; H, 3.91; N, 13.59.

Synthesis of Alkoxysilane Dyes (A1–A4). Alkoxysilane dyes (ASD, A1–A4) were synthesized by refluxing chromophores 1–4, respectively, for 48 h in THF solution containing ICTES with a small amount of triethylamine as catalyst. The products were precipitated from hexane and dried under vacuum.¹⁵

ASD A1. Yield: 69%. Mp = 123 °C. ¹H NMR (500 MHz, DMSO-*d*₆, ppm): 8.45 (d, ArH, 2H), 8.08 (d, ArH, 2H), 8.01 (d, ArH, 2H), 7.98 (s, NH, 1H), 7.38 (d, ArH, 2H), 3.77 (q, CH₂, 6H), 3.09 (q, CH₂, 2H), 1.56 (t, CH₂, 2H), 1.17 (t, CH₃,

9H), 0.61 (t, CH₂, 2H). Anal. Calcd for C₂₂H₃₀N₄O₇Si (490.3): C, 53.88; H, 6.12; N, 11.43. Found: C, 53.67; H, 6.05; N, 11.53.

ASD A2. Yield: 59%. Mp = 138 °C. ¹H NMR (500 MHz, DMSO-*d*₆, ppm): 8.45 (d, ArH, 2H), 8.05 (d, ArH, 2H), 7.87 (s, NH, 1H), 7.87 (s, ArH, 1H), 7.01 (s, ArH, 1H), 3.77 (q, CH₂, 6H), 3.06 (d, CH₂, 2H), 2.44 (s, CH₃, 6H), 1.54 (s, CH₂, 2H), 1.17 (t, CH₃, 9H), 0.60 (t, CH₂, 2H). Anal. Calcd for C₂₄H₃₄N₄O₇Si (518.7): C, 55.58; H, 6.60; N, 10.80. Found: C, 55.56; H, 6.61; N, 10.85.

ASD A3. Yield: 52%. Mp = 124 °C. ¹H NMR (500 MHz, DMSO-*d*₆, ppm): 8.42 (d, ArH, 2H), 8.05 (d, ArH, 2H), 7.90 (t, NH, 1H), 7.56 (s, ArH, 1H), 7.17 (s, ArH, 1H), 3.76 (q, CH₂, 6H), 3.07 (q, CH₂, 2H), 2.66 (s, CH₃, 3H), 2.16 (s, CH₃, 3H), 1.55 (t, CH₂, 2H), 1.16 (t, CH₃, 9H), 0.59 (t, CH₂, 2H). Anal. Calcd for C₂₄H₃₄N₄O₇Si (518.7): C, 55.58; H, 6.60; N, 10.80. Found: C, 55.34; H, 6.57; N, 10.77.

ASD A4. Yield: 47%. Mp = 151 °C. ¹H NMR (500 MHz, DMSO-*d*₆, ppm): 8.52 (d, ArH, 1H), 8.31 (q, ArH, 1H), 7.94 (t, NH, 1H), 7.79 (d, ArH, 1H), 7.56 (s, ArH, 1H), 7.21 (s, ArH, 1H), 3.76 (q, CH₂, 6H), 3.07 (q, CH₂, 2H), 2.68 (s, CH₃, 3H), 2.17 (s, CH₃, 3H), 1.55 (t, CH₂, 2H), 1.16 (t, CH₃, 9H), 0.60 (t, CH₂, 2H). Anal. Calcd for C₂₄H₃₃ClN₄O₇Si (553.1): C, 52.12; H, 6.01; N, 10.13. Found: C, 51.62; H, 5.88; N, 10.19.

Preparation of Hybrid Films (F1–F4). The alkoxysilane dyes were mixed with tetraethoxysilane (TEOS) at 1:3 molar ratio in THF; then acidic water (HCl, pH = 1) was added; the H₂O/Si molar ratio was 4:1. The solutions were stirred for 6 h and aged at room temperature for 7 days to increase viscosity. The sols were filtered through a 0.22 μm Teflon membrane filter and then spun-coated on the indium–tin–oxide (ITO) glass substrates to give inorganic–organic hybrid films (F1–F4).

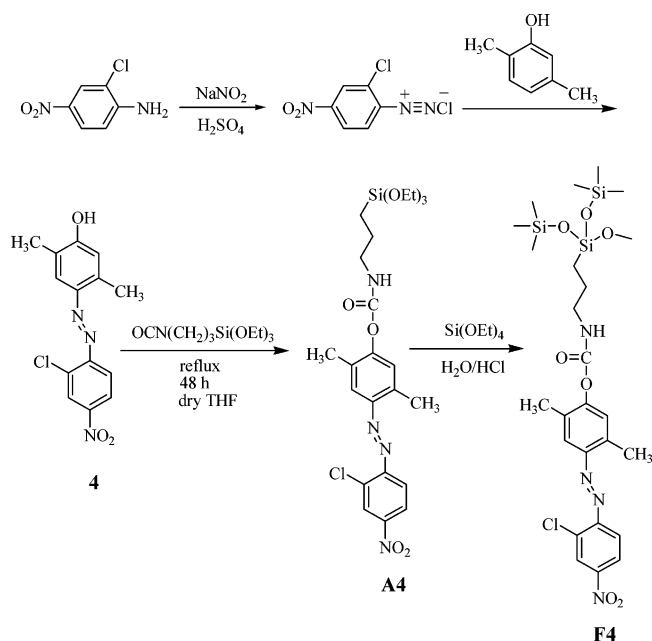
Second Harmonic Generation (SHG) Measurement. The second-order optical nonlinearity of hybrid films was determined by in situ SHG measurement. The laser source is a Q-switched Nd:YAG pulse laser with a 1064 nm P-polarized fundamental beam (500 mJ maximum energy, 3–5 ns pulse width, and 10 Hz repeating rate). The generated second harmonic signal was detected by a photomultiplier monitored by a monochromator to eliminate all traces of the fundamental light and processed by a Stanford Research Systems (SRS) model SR-250 gated integrator.

Characterization. FTIR spectra were recorded on a Nicolet Avatar 360 in the region of 4000–400 cm^{–1} using KBr pellets. The UV–visible absorption spectroscopic study was performed with a Perkin-Elmer Lambda 20 spectrophotometer. A Perkin-Elmer Pyris-1 thermogravimetric analyzer, with a heating rate of 20 °C/min up to 800 °C, was used for the thermal degradation study of samples under nitrogen atmosphere. The thickness and refractive index of the thin film was determined using the Metricon PC 2010 prism coupler at wavelengths of 632.8 and 1300 nm. Scanning electron microscopy (SEM, FEI SIRION 200) was used to study the morphology of the film (gold coated).

Results and Discussion

Synthesis and Characterization. The NLO chromophores (1–4) were synthesized through the traditional diazonium coupling reaction.^{16–18} Due to the weak basicity of 2-chloro-4-nitrobenzenamine, nitrosyl sulfuric acid was selected as a diazotizing agent because of its high reactivity in this reaction. The NLO chromophores were further reacted with ICTES to give functional sol–gel precursors (A1–A4) via a urethane forming reaction. Following the hydrolysis and copolymerization process of alkoxysilane dyes, four kinds of inorganic–organic

SCHEME 1: Synthetic Route of Hybrid Film F4



hybrid films (**F1–F4**) were prepared. The synthetic route of film **F4** is illustrated in Scheme 1 as an example.

The successful incorporation of chromophore into the silica network could be confirmed by FTIR spectra, as shown in Figure 2. In FTIR spectra, the films **F2–F4** showed two strong sharp peaks at about 1525 and 1343 cm^{-1} attributable to the asymmetric and symmetric stretching vibration of the nitro group in the chromophores, as well as a large absorption band around 1078 cm^{-1} due to an asymmetric Si–O–Si stretching vibration. The homogeneity of these inorganic–organic composites was further confirmed using SEM. The surface of the films did not have visible cracks, and no sign of any phase separation was observed when the magnification was increased to 10 000, as shown in Figure 3.

The analysis of the thermal properties was performed by thermogravimetric analysis (TGA) under a nitrogen atmosphere (see Figure 4). Due to the covalent linkage between the chromophore and silica backbone, all of the hybrid films (**F1–F4**) exhibited high thermal stability up to 290°C .

Measurement of $\beta_{\text{CT}}\mu_{\text{g}}$ Value for Chromophore. The UV–vis absorption spectra for the chromophores in THF are shown

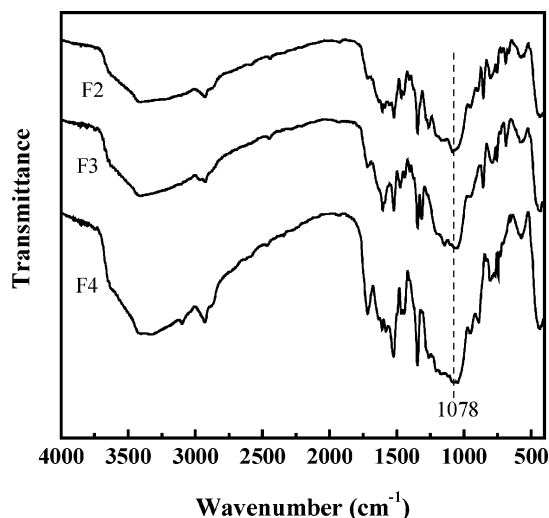


Figure 2. FTIR spectra of hybrid films **F2**, **F3**, and **F4**.

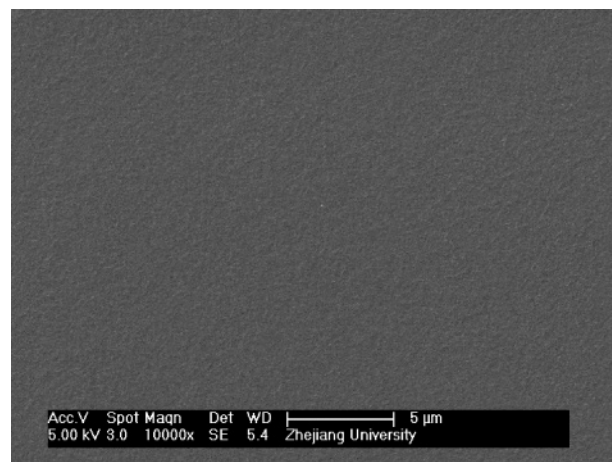


Figure 3. Scanning electron micrograph of hybrid film **F4**.

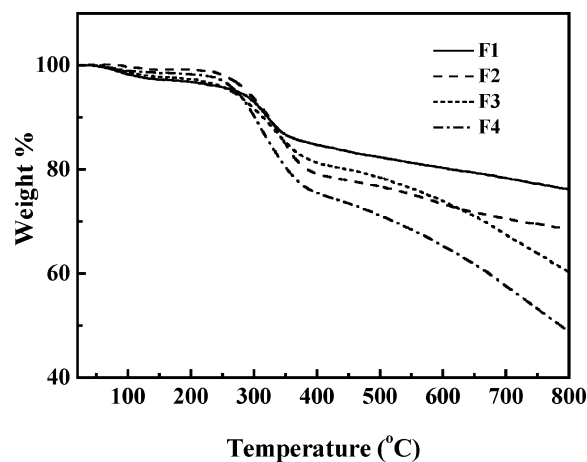


Figure 4. TGA trace for hybrid films **F1–F4**.

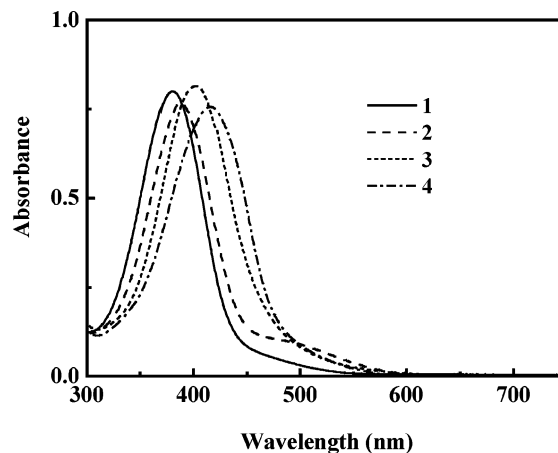


Figure 5. UV–visible absorption spectra of chromophores **1–4** in THF.

in Figure 5. All of them exhibited good transparency in the visible range. Relative to chromophore **1**, the two-methyl substituent **2** has a red shift of 9 nm , and the others are more bathochromic than **2**. Chromophore **4**, which has two methyls and a chloric groups, causes the largest red shift of 36 nm relative to **1**. Generally, for the donor– π –acceptor system, strong electron-withdrawing ability can cause large bathochromic shift, and this bathochromic shift is beneficial to give large NLO response.

The $\beta_{\text{CT}}\mu_{\text{g}}$ values of chromophores were evaluated by a solvatochromic method, which is based on the solvent depen-

TABLE 1: Experimental Data of the Chromophores in Solvatochromic Measurement

chromophore	λ_{\max}^a (nm)	ϵ (10^4 $\text{mol}^{-1} \cdot \text{L} \cdot \text{cm}^{-1}$)	$\Delta\nu_{1/2}$ (cm^{-1})	λ_{\max}^b (nm)	$\Delta\nu$ (cm^{-1})	$\beta_{\text{CT}}\mu_{\text{g}}$ (10^{-30} $\text{esu} \cdot \text{D}$)
1	387	2.35	5261	381	407	141.2
2	391	2.36	5152	381	671	242.4
3	407	2.61	5380	396	683	361.1
4	421	2.59	5835	413	460	325.3

^a Measured in DMF. ^b Measured in CHCl_3 .

dence of the UV–vis absorption spectrum of a molecule. As previously described in the literature,^{19,20} the values of $\beta_{\text{CT}}\mu_{\text{g}}$ can be found as follows:

$$\beta_{\text{CT}}\mu_{\text{g}} = (4.612 \times 10^{-5}) \frac{f(\lambda)\epsilon\Delta\nu_{1/2}\Delta\nu\lambda^3}{\Delta f(D)}$$

$$f(\lambda) = \frac{\lambda^3\lambda_0^4}{(\lambda_0^2 - 4\lambda^2)(\lambda_0^2 - \lambda^2)}$$

$$f(D) = \frac{2(D-1)}{2D+1} \quad (1)$$

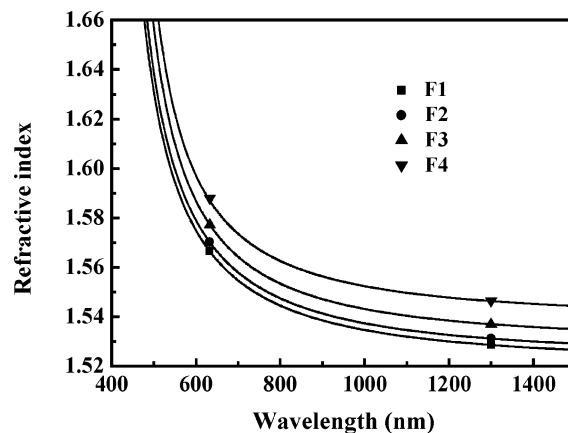
where λ is the maximum absorption wavelength of the molecule in an excited state and, here, it is assumed to be the maximum absorption wavelength of the molecule in dipolar solvent; ϵ , $\Delta\nu_{1/2}$, $\Delta\nu$, and λ_0 are the maximum of the absorption coefficient in dipolar solvent, the difference of the width of peaks at the middle, the shift of the maximum absorption in different solvents, and the wavelength of the base frequency, respectively. The cgs unit system is adopted; the unit of ϵ is $\text{mol}^{-1} \cdot \text{L} \cdot \text{cm}^{-1}$ and the unit of D is debye. The $\beta\mu$ values for chromophores 1–4 at the wavelength of 1064 nm are listed in Table 1.

The chromophores 2 and 3 exhibit much larger β values than 1 due to their higher electronic donor strength. Compared with chromophore 2, chromophore 3 has same kind of conjugated bridge and substituent groups but different substituent position. Chromophore 3 shows a larger β value than 2. This result can be explained by considering the chromophore structure. Cheng et al. have shown the substitution pattern effect in disubstituted stilbene on charge-transfer interactions between the donor and acceptor groups. They concluded that the β value of the different substituent positions were in the order of para > ortho > meta, and in the case of weak donors such as methyl group, the order was para > meta > ortho.^{21,22} It is also reasonable to accept the conclusion in these azobenzene molecules. The two methyl groups of chromophore 2 were in the ortho position of the azobenzene group, which did not allow strong charge-transfer strength between donor and acceptor and might have decreased its β value. For chromophore 4, which has a nitro and a chloric group acting as acceptor, the β value is near that of 3. The result evidenced once more that the substituent group in the ortho position could not bring considerable improvement in β value.

Linear and Nonlinear Optical Properties of Films. The refractive index (RI) and thickness for the hybrid films are measured using the prism coupling method at wavelengths of 632.8 and 1300 nm. The wavelength dispersion of RI, $n(\lambda)$, can be fitted to a one-oscillator Sellmeier-dispersion formula,²³

$$n^2(\lambda) - 1 = \frac{q}{1/\lambda_0^2 - 1/\lambda^2} + A \quad (2)$$

where λ_0 is the absorption wavelength of the dominant oscillator, q is a measure for the oscillator strength, and A is a constant

**Figure 6.** Dispersion of the refractive index of hybrid films F1–F4.**TABLE 2: Linear and Nonlinear Optical Properties of Hybrid Films**

hybrid film	thickness (μm)	refractive index		d_{33} (pm/V)
		532 nm	1064 nm	
F1	1.14	1.605	1.533	3.4
F2	0.99	1.611	1.536	5.6
F3	1.32	1.623	1.541	8.9
F4	1.06	1.637	1.551	14.3

containing the sum of all the other oscillators. Figure 6 shows the curve of RI using eq 2. Thickness and RI values at 532 and 1064 nm obtained from the plot are listed in Table 2.

The noncentrosymmetric alignment of the chromophores, which was essential for second-order optical nonlinearity, was achieved by corona poling, and the in situ SHG was used to probe the nonlinearity of the films. The corona voltage (5.5 kV) was applied from room temperature; when the temperature was raised to 150–170 °C, the SHG intensity increased to the maximum. The poling field was kept for 30 min at the optimum poling temperatures and then removed after the film cooled to room temperature. The second harmonic intensity was measured using p (parallel-polarized) excitation and p detection and compared with the second harmonic generated by a Y-cut quartz crystal. Calculation of the second harmonic coefficients (d_{33}) for the poled films was based the following equation:^{24–27}

$$\frac{d_{33,s}}{d_{11,q}} = \sqrt{\frac{I_s L_{\text{qc}}}{I_q L_s}} F \quad (3)$$

where the $d_{11,q}$ is d_{11} of the quartz crystal, which is 0.5 pm/V. I_s and I_q are the SHG intensities of the sample and the quartz, respectively. L_{qc} is the coherent length of the quartz, which is 20.6 μm , L_s is the thickness of the films, and F is the correction factor of the apparatus and equals 1.2 when $L_{\text{qc}} \gg L_s$. The d_{33} values of the poled film are calculated at 1064 nm fundamental wavelength and listed in Table 2. The poled film F3, with the highest molecular hyperpolarizability (β), does not exhibit the highest d_{33} value, and the film F4 shows the highest d_{33} among the four poled films. The possible reason is that the introduction of a chloric substituent group might prevent the aggregation of the chromophores, which results in the higher d_{33} value for film F4.

As far as NLO devices are concerned, the thermal stability of the poled films is of paramount importance. The stability of optical nonlinearity was investigated through a depoling experiment in which the SHG signal was monitored as the poled film was heated at a rate of 10 °C/min from 30 to 200 °C. F4 was selected as the typical sample, and its plot of SHG signal vs

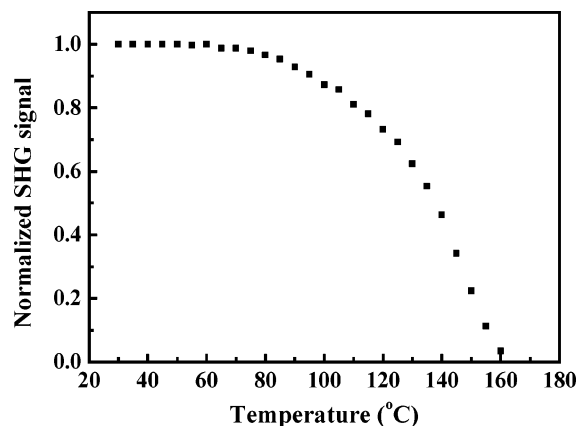


Figure 7. Decay of the SHG signal as a function of temperature for hybrid film F4.

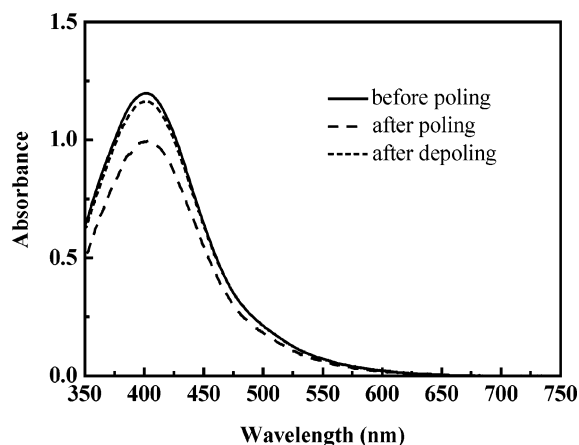


Figure 8. UV-vis absorption spectra of hybrid film F4 before poling, after poling, and after depoling.

temperature is shown in Figure 7. It can be seen that the decay onset of the SHG signal occurred at around 90 °C, and its half-decay temperature was at about 140 °C.

To investigate the thermal stability of the chromophore under the heating condition, we compared the absorption spectrum of the film F4 before poling, after poling, and after depoling. As seen in Figure 8, poling causes a decrease of absorption intensity and a shorter wavelength shift of the absorption maximum, which is the result of the alignment of the chromophore dipoles. The order parameter ϕ ($\phi = 1 - A_1/A_0$, A_0 and A_1 are absorbances of the film before and after poling) was calculated to be 0.19, which was used to characterize the poling efficiency.²⁸ After the depoling experiment, the absorption spectrum of the film was almost recovered. We can conclude that the decomposition or sublimation of the chromophore did not occur during the poling and depoling process.

Conclusions

We have presented a series of azobenzene chromophores, where different substituent groups are incorporated in the conjugated bridge. The chromophore-attached precursors were successfully synthesized through a nucleophilic addition reaction

and further by a sol–gel process to give the inorganic–organic hybrid films. The nonlinear optical activities (d_{33}) of thin hybrid films were evaluated by in situ SHG to be about 5–15 pm/V. We also discuss the influences of substituent groups and substituent position on $\beta_{CT}\mu_g$ values and d_{33} values. These hybrid films exhibit excellent transparency in the visible range, indicating their suitability for double-frequency device applications in the blue and green regions.

Acknowledgment. The authors gratefully acknowledge the financial support for this work from the National Natural Science Foundation of China (under Grant No. 50532030), the Foundation for the Author of National Excellent Doctoral Dissertation of P. R. China (Grant No. 200134), and Education Foundation of FOK Ying Tung (Grant No. 81042).

References and Notes

- (1) Zyss, J. *Molecular Nonlinear Optics Materials Physics and Devices*; Academic Press: Orlando, FL, 1994.
- (2) Prasad, P. N.; Williams, D. J. *Introduction to Nonlinear Optical Effects in Molecules and Polymers*; John Wiley & Sons, Inc.: New York, 1991.
- (3) Sandhya, K. Y.; Chennakattu, K. S. P.; Naoto, T. *Prog. Polym. Sci.* **2004**, *29*, 45.
- (4) Lee, J. Y.; Bang, H. B.; Park, E. J.; Baek, C. S.; Rhee, B. K.; Lee, S. M. *Synth. Met.* **2004**, *144*, 159.
- (5) Jeng, R. J.; Chang, C. C.; Chen, C. P.; Chen, C. T.; Su, W. C. *Polymer* **2003**, *44*, 143.
- (6) Yesodha, S. K.; Sadashiva; Pillai, C. K.; Jsutsumi, N. *Prog. Polym. Sci.* **2004**, *29*, 45.
- (7) Jeon, B. J.; Cha, S. W.; Jeong, M. Y.; Lim, T. K.; Jim, J. J. *Mater. Chem.* **2002**, *12*, 546.
- (8) Zhang, H. X.; Lu, D.; Fallahi, M. *Appl. Phys. Lett.* **2004**, *84*, 1064.
- (9) Chaumel, F.; Jiang, H. W.; Kakkar, A. *Chem. Mater.* **2001**, *13*, 3389.
- (10) Kim, H. K.; Kang, S. J.; Choi, S. K.; Min, Y. H.; Yoon, C. S. *Chem. Mater.* **1999**, *11*, 779.
- (11) Hsiue, G. H.; Lee, R. H.; Jeng, R. J. *Chem. Mater.* **1997**, *9*, 883.
- (12) Ledoux, I.; Zyss, J.; Barni, E.; Barolo, C.; Diulgheroff, N.; Qualiotto, P.; Viscardi, G. *Synth. Met.* **2000**, *115*, 213.
- (13) Qiu, L.; Shen, Y. Q.; Hao, J. M.; Zhai, J. F.; Zhao, Y. X.; Clays, K.; Persoons, A. J. *Mater. Sci.* **2004**, *39*, 2335.
- (14) He, M. Q.; Leslie, T. M.; Sinicropi, J. A. *Chem. Mater.* **2002**, *14*, 4662.
- (15) Cui, Y. J.; Wang, M. Q.; Chen, L. J.; Qian, G. D. *Dyes Pigm.* **2005**, *65*, 61.
- (16) Tang, H. D.; Liu, Y. Y.; Huang, B.; Qin, J. G.; Fuentes-Hernandez, C.; Kippelen, B.; Li, S. J.; Ye, C. J. *Mater. Chem.* **2005**, *15*, 778.
- (17) Jung, G. B.; Honda, K.; Mutai, T.; Matoba, O.; Ashihara, S.; Shimura, T.; Araki, K.; Kuroda, K. *Jpn. J. Appl. Phys.* **2003**, *42*, 2699.
- (18) Sandhya, K. Y.; Pillai, C. K. S.; Sato, M.; Tsutsumi, N. *Macromol. Chem. Phys.* **2002**, *203*, 1126.
- (19) Song, H. C.; Chen, Y. W.; Zheng, X. L.; Ying, B. N. *Spectrochim. Acta, Part A* **2001**, *57*, 1717.
- (20) Bilot, V. L.; Kaski, A. Z. *Naturforsch. A* **1962**, *17*, 621.
- (21) Sung, P. H.; Chen, C. Y.; Wu, S. Y.; Huang, J. Y. *J. Polym. Sci.: Part A* **1996**, *34*, 2189.
- (22) Cheng, L. T.; Tam, W.; Mander, S. R.; Stiegman, A. E.; Rikken, G.; Spargler, C. W. *J. Phys. Chem.* **1991**, *95*, 10643.
- (23) Naoto, T.; Mikio, M.; Wataru, S. *Macromolecules* **1998**, *31*, 7764.
- (24) Dalton, L. R.; Xu, C.; Harper, A. W.; Ghson, R.; Wu, B.; Liang, Z.; Montgomery, R.; Jen, A. K.-Y. *Nonlinear Opt.* **1995**, *10*, 383.
- (25) Pan, Q. W.; Fang, C. S.; Qin, Z. H.; Gu, Q. T.; Cheng, X. F.; Xu, D.; Yu, J. Z. *Mater. Lett.* **2003**, *57*, 2612.
- (26) Lu, Z. Q.; Shao, P.; Li, J.; Hua, J. L.; Qin, J. G.; Qin, A. J.; Ye, C. *Macromolecules* **2004**, *37*, 7089.
- (27) Luo, J. D.; Qin, J. G.; Kang, H.; Ye, C. *Chem. Mater.* **2001**, *13*, 927.
- (28) Mortazavi, M. A.; Knoesen, A.; Kowel, S. T.; Higgins, B. G.; Dienes, A. J. *Opt. Soc. Am. B* **1989**, *6*, 733.